KRONOS FUSION ENERGY

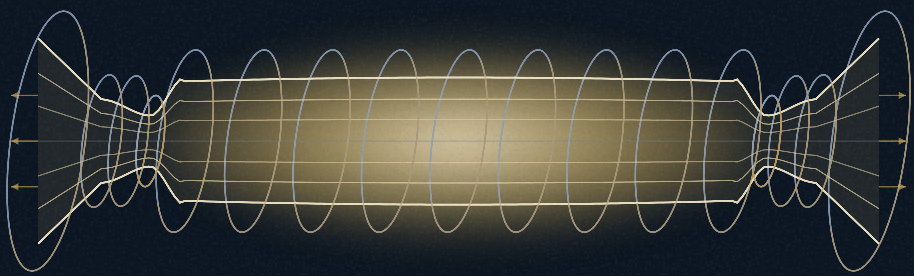

PAPER 2.52 · THE KRONOS 2026 SERIES

Tandem-Mirror Design-Space Mapping for a D–^{3}He Burner: 0-D Power Balance Benchmarked against WHAM and the Pastukhov-Plug Operating Point

A D–He tandem mirror trades the closed field lines of a torus for an open, linear geometry whose engineering gain is set not by confinement time alone but by the ambipolar…

Read it live — 3-D model · physics validator · film series

BY P I FORD AND G L KULCINSKI

2026 · EDITORIAL EDITION

THE OFFICIAL RECORD

What this document is, and how to read its numbers

This is a combined editorial. It gathers, in one volume, the two design studies Kronos Fusion Energy released in 2026 — a compact spherical-tokamak tritium/helium-3 breeder and a deuterium–helium-3 tandem-mirror generator — together with the intellectual-property estate, the people, and, in the internal edition, the full commercial case. The scientific text is the same text that appears in the arXiv preprints and the journal submissions; the editorial adds the apparatus a reader needs to hold the whole program at once, and nothing in the physics is altered to fit it.

THE HONESTY STANCE IS THE ASSET

Every headline quantity carries an **evidence class** — DERIVED RECOMPUTED MEASURED REQUIREMENT — and, where a number is a modelled extrapolation rather than a demonstrated value, it is labelled as such and its downside is shown next to it. Several quantities in the underlying corpus moved after first publication; where a value has been withdrawn or restated, the record says so plainly. This is deliberate: a diligence team will find the load-bearing assumptions, so the document surfaces them first.

TWO EDITIONS

This volume is issued in two editions. The **public edition** (light) carries the physics and the design only — no dollar, price, or per-kilogram figure appears anywhere in it. The **internal edition** (dark) adds the economics, the funding architecture, and the defense-commercial analysis, and is marked *Confidential* accordingly; it is not for public distribution. Where the commercial case rests on a modelled assumption rather than a demonstrated one, it is labelled as such and its downside is shown alongside it, on the same terms as the physics.

TITLE	The Kronos Fleet — Hyperion · Aegis · MetroVolt: A Combined Design & Commercialization Study
AUTHOR	Priyanca Ford, Founder & CEO, on behalf of Kronos Fusion Energy
EDITION	2026 Combined Editorial · first issue
COMPANION WORKS	The five-paper arXiv drop — (1) Breeder, (2) Burner, (3) REBCO magnet & tape, (4) Direct Energy Conversion, (5) AI/ML/Quantum control — with matching numbered Zenodo deposits, plus the IOP journal and IAEA-FEC submissions. Patents were filed before the drop.
NAMING	Hyperion = the breeder; Aegis (defense) and MetroVolt (data-center) = one generator in two housings. Internal mode letters (D1, L) do not appear on public surfaces.
STATUS	Conceptual design & simulation study. Nothing herein is a construction commitment.

HOW TO READ THIS VOLUME

The fleet at a glance, and the way its numbers are marked

This volume opens with *Orientation*, presents the five research papers as a bound sequence, and closes with the *Apparatus*. *Foundations* sets out the three general results both machines rest on. *Paper One* is the Hyperion breeder; *Paper Two* the Aegis / MetroVolt generator; *Papers Three, Four and Five* are the enabling science — high-field REBCO magnets and tape, direct energy conversion, and the AI / ML / quantum control stack. A *Digital Twin & 3-D Model* part follows, then the *Environmental* profile. The *Economics* and levelized cost and the *Business Case* and diligence record appear in the internal edition only; the *Simulations* proof record and the Apparatus — patent portfolio, team, limitations, and sources — close both editions.

THE FLEET AT A GLANCE

	HYPERION	AEGIS	METROVOLT
Role	Strategic-isotope foundry	Defense installation power	Campus power
Machine	**Spherical tokamak**	**Tandem mirror**	**Tandem mirror**
Fuel	Deuterium–tritium	Deuterium–helium-3	Deuterium–helium-3
Delivers	Tritium · ^{3}He · 14 MeV n	Resilient installation power	Firm campus power
Physics bar	**Fusion gain only**	Closure (gates named)	Closure + lunar ^{3}He
In the fleet	Breeds the fuel	Proves the generator	Commercial destination

HOW THE NUMBERS ARE MARKED

Every headline quantity carries an evidence class — DERIVED from first principles, RECOMPUTED from raw data, MEASURED in hardware, or a REQUIREMENT yet to be met. Financial figures carry a case label and are confined to the internal (confidential) edition. Values that moved after first publication are shown as withdrawn or restated rather than quietly changed. A capability you can evaluate is one whose limits are on the page.

ABSTRACT

Tandem-Mirror Design-Space Mapping for a D–^{3}He Burner: 0-D Power Balance Benchmarked against WHAM and the Pastukhov-Plug Operating Point

A D–^{3}He tandem mirror trades the closed field lines of a torus for an open, linear geometry whose engineering gain is set not by confinement time alone but by the ambipolar potential a high-field plug can hold. We map the design space of the Kronos burner with a zero-dimensional power balance closed by a Pastukhov–Fokker–Planck end-loss model, deriving the governing equations from the mirror loss cone, the Boltzmann plug potential, and the central-cell power budget, and solving them on a verified evaluator run on the NVIDIA GPU high-performance-computing (HPC) campaign. At the frozen reference point the balance closes at engineering gain $Q_E = 1.318$, fusion power $P_{\text{fus}} = 4298.5$ MW of which only a neutron fraction $f_n = 5.44\%$ is carried by neutrons ($P_n = 233.95$ MW), an ambipolar plug potential $\varphi_i = 248.75$ keV ($e\varphi_i/T_i = 2.764$) sustained at a plug density ratio $n_{\text{plug}}/n_c = 16$ behind a 26.49 T plug coil, and a direct-energy-conversion (DEC) efficiency at the frozen conservative anchor $\eta_{\text{DEC}} = 0.49$. Sampling the density–temperature plane produces a net-gain database in which *all 25 of 25 feasible samples clear* $Q_E > 1$ over $Q_E = 1.107$–1.414, with a robust ion-temperature ridge near 85 keV and the reference point in the feasible interior; a 40 000-sample global Monte-Carlo returns $Q_E = 1.317 \pm 0.14$ with $P(Q_E > 1) = 1.0$. A Saltelli–Sobol analysis ranks the plug density ratio as the leading first-order driver ($S_1 = 0.41$), coupled to central-cell β through interactions ($S_T = 0.87$); we show this follows analytically from the exponential dependence of the Pastukhov confinement on $\ln(n_{\text{plug}}/n_c)$. One physics scales across two housings: the balance closes at $+104$ MWe net for a 55 m unit and $+850$ MWe net for a 440 m unit. A direct benchmark against the Wisconsin HTS Axisymmetric Mirror (WHAM) reproduces its measured *unplugged* fields, kilo-volt-class potential and neutron rate, and shows the plugged closure to be conservative there by two to three orders; the plugged net-gain branch itself is the single well-posed quantity a plugged-mirror experiment must confirm. The burner therefore enters detailed design with a demonstrated, sensitivity-ranked operating window and one identified experimental checkpoint.

Open-access deposit (code & data, CC BY 4.0): DOI 10.5281/zenodo.22645911 · Zenodo community *kronos_fusion_energy*. Explore it live: interactive 3-D model · physics validator.

Keywords: tandem mirror · Pastukhov plug · ambipolar potential · D--^{3}He · direct energy conversion · net electric gain · design-space database · global sensitivity · WHAM benchmark

CONTENTS

Table of Contents

NOMENCLATURE

Symbols, units, and the names of things

Q	plasma (fusion) gain, P_{fus}/P_{aux}
Q_E	engineering gain, net electric out / recirculating in
H_{98}	confinement enhancement over the IPB98(y,2) scaling
Z_{eff}	effective ion charge
c_{ee}	electron–electron bremsstrahlung leading coefficient, 2.120022 (exact)
τ_E	energy confinement time
I_p	plasma current
R_0, a	major radius, minor radius
κ, δ	elongation, triangularity
β_N	normalized plasma beta (Troyon-normalized)
TBR	tritium breeding ratio
DEC	direct energy conversion
CF	plant capacity factor (availability)
FOAK / NOAK / BOAK	first / n^{th} / best of a kind
Hyperion	the ST breeder (internal: Mode D2)
Aegis	the generator, defense/installation housing (internal: Mode M)
MetroVolt	the generator, data-center housing (Mode M)

tandem mirror; Pastukhov plug; ambipolar potential; D–^{3}He; direct energy conversion; net electric gain; design-space database; global sensitivity; WHAM benchmark

§ 1

Introduction

OPEN SYSTEMS AND THE KRONOS BURNER

A magnetic mirror confines a plasma between two regions of intensified field, so that particles whose velocity lies outside a loss cone are reflected and the rest stream out along the open field lines [1,2]. The appeal of the geometry is engineering, not merely physical: an open, axisymmetric device is linear, has no toroidal field-coil interlinking, converts its escaping charged-particle power directly to electricity on the fanned field lines of an expander [3], and–because it need not sustain a large bootstrap current–recirculates a low fraction of its output. The historic liability of the simple mirror is that collisional scattering fills the loss cone: absent an extra confining mechanism, the parallel confinement time is only of order the ion–ion collision time, and the fusion gain is small. The *tandem* mirror of Dimov and of Fowler and Logan [4,5] removes that liability by placing high-field, high-density end plugs that build a positive ambipolar potential, electrostatically confining the central-cell ions between two potential hills [6]. The confinement of the central cell then rises exponentially with the depth of that potential, and the machine's gain is set by how deep a potential the plug can hold.

The Kronos burner is a D–^{3}He tandem mirror designed around exactly this trade. Its central cell operates at $T_i \approx 90$ keV behind mirror throats at 17 T, and it is plugged by a pair of no-insulation REBCO plug coils that reach a peak field of 26.49 T [27]. Two housings share the identical physics and diverge only at balance of plant–a fixed forward-base unit (Aegis) [26] and a data-centre unit (MetroVolt)–so that the same power balance describes both. The reference point delivers net electric gain: engineering gain $Q_E = 1.318$ at fusion power $P_{\text{fus}} = 4298.5$ MW, with only $f_n = 5.44\%$ of that power carried by neutrons and the 14.68 MeV proton branch of the D–^{3}He reaction recovered directly at a conversion efficiency held, in the frozen anchor, to a deliberately conservative $\eta_{\text{DEC}} = 0.49$ [28].

THE QUESTION THIS PAPER ANSWERS

A single operating point is not a design. Before a burner program commits, it must show three things: that net gain is the interior of a broad feasible box rather than a knife-edge optimum; that the physical levers controlling the gain are identified and ranked, so the pacing subsystem is known; and that the model is benchmarked against the one operating machine in its class, with the residual physics stated plainly rather than diffused across the whole device. This paper establishes all three for the Kronos burner. We derive the governing equations from first principles (§2), give the numerical formulation and the GPU-HPC campaign that produced the results (§3), and then present, in turn, the reference power balance, the 25-point net-gain database and its 40 000-sample uncertainty quantification, the global-sensitivity ranking, the DEC-efficiency ladder, the two-housing power-class scaling, and the WHAM benchmark (§4). Every quantitative claim traces to a frozen result in the Kronos Physics De-Risking Register [25]; the serial identifiers (e.g. BU-L1-A1) are given inline so each number is auditable.

PRIOR ART AND CONTRIBUTION

The physics we assemble is individually classical. Pastukhov gave the collisional loss rate of a species confined in a mirror by an electrostatic potential [7]; Cohen, Rognlien and Baldwin and later Najmabadi, Conn and Cohen refined the closure into the form used in tandem-mirror reactor studies [8,9]. The tandem-mirror confinement principle was demonstrated with kilovolt-class plug potentials on TMX-U and GAMMA-10 [10,11], and Fowler, Moir and Simonen have argued that a high-field, sloshing-ion plug returns the tandem mirror to a simple, high-gain configuration [12]. Direct energy conversion of mirror end-loss was measured on the venetian-blind and later converters of Moir and Barr [3,13], and the low-neutron D–^{3}He fuel cycle has a long analysis literature [14,15]. What has been missing for a specific compact burner is a single, verification-grounded synthesis: a power balance whose every anchor is independently reproduced, mapped across its operating plane, ranked by global sensitivity, tied to the plug physics through an explicit analytic argument, and benchmarked against a real high-field mirror with the modelled-versus-measured boundary drawn honestly. That synthesis is the contribution here. It complements the companion studies that resolve the individual subsystems–the 26.49 T plug coil [27], the sloshing-ion ambipolar potential [29], the DCLC/AIC microstability of the warm-fill [30], the synchrotron-pinned electron temperature [31], the recirculation-resolved gain closure [32], and the cross-machine global uncertainty quantification [33]–and places them on a common, sensitivity-mapped operating window.

§ 2

Governing equations and the formal problem

The burner power balance is a zero-dimensional (0-D) model of a single flux tube through the central cell, closed by a kinetic end-loss law. We build it in four steps: the mirror loss cone, the ambipolar plug potential, the Pastukhov end-loss closure, and the central-cell power budget; we then state the engineering gain and the formal design-space problem.

THE MIRROR LOSS CONE AND THE ADIABATIC INVARIANT

In the slowly varying field of the mirror the magnetic moment $\mu = mv_\perp^2/2B$ is an adiabatic invariant, and with energy $\frac{1}{2}m(v_\parallel^2 + v_\perp^2)$ conserved a particle launched from the field minimum B_{min} is reflected before the field maximum B_{max} provided its pitch angle $\theta = \arctan(v_\perp/v_\parallel)$ exceeds the loss-cone angle

$$\sin^2\theta_{\text{lc}} = \frac{B_{\text{min}}}{B_{\text{max}}} = \frac{1}{R_m}, \qquad R_m \equiv \frac{B_{\text{max}}}{B_{\text{min}}},$$

where R_m is the mirror ratio. At the reference point the effective confining ratio is $R_m = 4.61$, giving a loss-cone half-angle $\theta_{\text{lc}} = 27.77°$ (BU-L2-A2, SC-BU-2). A Maxwellian without an electrostatic barrier would empty its loss cone on the ion–ion scattering time, so the loss cone alone confines only weakly; the plug potential is what suppresses it.

THE AMBIPOLAR PLUG POTENTIAL

Electrons, being far more collisional and mobile than ions, escape the plug faster; charge quasineutrality forces a positive electrostatic potential to build until the electron loss is throttled to the ion loss. In the high-density plug (n_{plug}) relative to the central cell (n_c) the electrons obey a Boltzmann relation along the field line, $n_c/n_{\text{plug}} = \exp(-e\varphi_c/T_e)$, so the potential peak seen by a central-cell ion is

$$\frac{e\varphi_i}{T_i} \simeq \ln\left(\frac{n_{\text{plug}}}{n_c}\right).$$

At the design ratio $n_{\text{plug}}/n_c = 16$ this gives $e\varphi_i/T_i \simeq \ln 16 = 2.773$, in agreement with the frozen evaluator value $e\varphi_i/T_i = 2.764$ ($\varphi_i = 248.75$ keV at $T_i \approx 90$ keV; BU-L1-A1). The logarithmic dependence in equation (2) is the analytic root of the sensitivity ranking derived in §4.4: the potential depth–and, through the exponential below, the confinement–is set by the plug density ratio. The self-consistent formation of φ_i by hot electrons and sloshing ions is treated kinetically in the companion study [29]; here it enters as the closure (2).

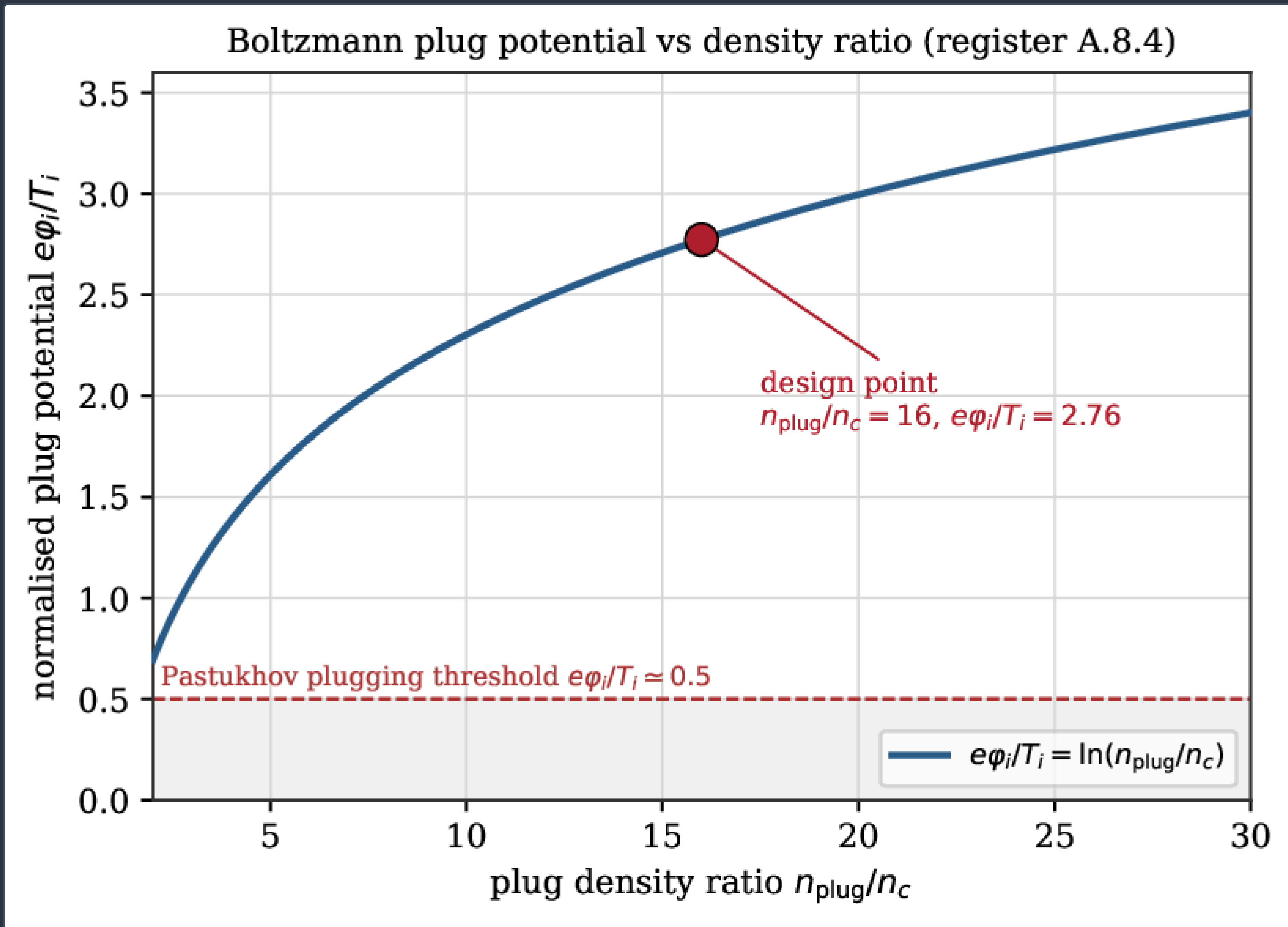

The Boltzmann plug potential versus plug density ratio, equation (2). The design point ($n_{\rm plug}/n_c = 16$, $e\varphi_i/T_i = 2.76$) sits well above the Pastukhov plugging threshold ($e\varphi_i/T_i \simeq 0.5$, shaded); the logarithmic dependence is the analytic origin of the sensitivity ranking of §4.4.

THE PASTUKHOV–FOKKER–PLANCK END-LOSS CLOSURE

An ion confined in the central cell by the barrier $e\varphi_i$ escapes only when pitch-angle scattering carries it across the barrier and into the loss cone. Solving the Fokker–Planck equation for the loss rate over a potential well, Pastukhov [7]–as refined by Cohen, Rognlien and Baldwin [8] and Najmabadi, Conn and Cohen [9]–gives a parallel confinement time of the form

$$\tau_\parallel \;=\; \tau_{ii}\,\sqrt{\pi}\,g(R_m)\;\hat\varphi\,e^{\hat\varphi}, \qquad \hat\varphi \equiv \frac{e\varphi_i}{T_i}, \qquad g(R_m) = \frac{2R_m+1}{2R_m}\,\ln(4R_m+2),$$

with the ion–ion 90° collision time

$$\tau_{ii} = \frac{12\,\pi^{3/2}\,\varepsilon_0^2\,\sqrt{m_i}\,T_i^{3/2}}{\sqrt{2}\,n_i\,Z^4 e^4\,\ln\Lambda}.$$

The decisive feature of equation (3) is the factor $\hat\varphi\,e^{\hat\varphi}$: confinement rises *exponentially* in the normalised potential, and hence–through equation (2)–exponentially in $\ln(n_{\rm plug}/n_c)$, i.e. linearly in the density ratio itself. At the reference point ($\hat\varphi = 2.764$, $R_m = 4.61$) the enhancement is $\hat\varphi e^{\hat\varphi} \approx 43.8$ and $g(R_m) \approx 3.34$, and the evaluator returns a plugged confinement time $\tau_p = 3.73$ s (BU-L1-A1)–more than two orders of magnitude above the unplugged scattering time. Equation (3) is valid only for a genuine barrier, $\hat\varphi \gtrsim 0.5$; below that the potential no longer plugs and the expression must not be applied, a point that governs the WHAM benchmark of §4.7.

THE CENTRAL-CELL POWER BUDGET

The 0-D fusion power density in the central cell sums over reacting pairs,

$$p_{\text{fus}} = \sum_{a \le b} \frac{n_a n_b}{1+\delta_{ab}} \langle \sigma v \rangle_{ab}(T_i)\, E_{ab},$$

with Maxwellian-averaged reactivities $\langle \sigma v \rangle_{ab}(T_i)$ evaluated from the Bosch–Hale parametrisation [18]. The dominant channel is

$$\text{D} + {}^3\text{He} \;\rightarrow\; p\,(14.68\ \text{MeV}) + \alpha\,(3.67\ \text{MeV}),$$

whose 18.35 MeV are entirely charged and therefore directly convertible; the parasitic $\text{D}+\text{D}$ branches (and the $\text{D}+\text{T}$ burn of the tritium they breed) supply the only neutrons. At the reference point $P_{\text{fus}} = 4298.5$ MW, of which the D–^{3}He channel carries $P_{\text{D}^3\text{He}} = 3868.0$ MW and the D–D side reactions the balance, so that the neutron power is $P_n = 233.95$ MW and the neutron fraction

$$f_n \equiv \frac{P_n}{P_{\text{fus}}} = 5.44\%,$$

an order of magnitude below a D–T system and the origin of the machine's neutron-lean siting case. The charged power is depleted by radiation–bremsstrahlung $p_{\text{br}} \propto n_e^2 Z_{\text{eff}} \sqrt{T_e}$ with $Z_{\text{eff}} = 1.462$, and cyclotron radiation, which at the high field and high T_e of the plug is significant and pins the electron temperature through re-absorption and transport [31]. The surviving charged power flows out of the mirror ends to the direct converters.

ENGINEERING GAIN AND THE FORMAL DESIGN-SPACE PROBLEM

The engineering gain is the ratio of gross electric output to recirculated electric input,

$$Q_E \equiv \frac{P_{\text{out}}}{P_{\text{in}}}, \qquad P_{\text{out}} = \eta_{\text{DEC}}\, P_{\text{ch}}^{\text{ax}} + \eta_{\text{th}}\, P_{\text{th}}, \qquad P_{\text{net}} = P_{\text{out}} - P_{\text{in}},$$

where $P_{\text{ch}}^{\text{ax}}$ is the axial charged-particle power reaching the DEC, P_{th} the thermally recovered remainder (neutrons, radiation and non-axial loss), and P_{in} the wall-plug power that sustains the plasma and the plug. Net electric gain requires $Q_E > 1$; at the reference point $P_{\text{out}} = 3522.0$ MWe and $P_{\text{in}} = 2672.0$ MWe give $P_{\text{net}} = +850.0$ MWe and $Q_E = 1.318$ (BU-L1-A1). The design task is to maximise the gain over the operating variables subject to the physics constraints,

$$\begin{aligned} \max_{n_c,\, T_i,\, n_{\text{plug}}/n_c,\, \beta_c} \quad & Q_E(n_c, T_i, n_{\text{plug}}/n_c, \beta_c) & \\ \text{s.t.} \quad & \hat{\varphi} = \ln(n_{\text{plug}}/n_c) \gtrsim 0.5 & \text{(plug validity)}, \\ & \beta_c \le \beta_c^{\max} & \text{(central-cell MHD)}, \\ & B_{\text{plug}} \le 26.49\ \text{T} & \text{(plug-coil field limit)}, \\ & \text{warm-fill} \;\ge f_{\text{DCLC}} & \text{(loss-cone microstability)}, \\ & p_{\text{rad}} \le p_{\text{rad}}^{\text{ceiling}} & \text{(radiation ceiling)}. \end{aligned}$$

The remainder of the paper characterises the feasible set of equation (9): its interior (the net-gain database), its dominant active constraint (the plug, via global sensitivity), and the one constraint whose quantitative form is not yet measured (plug validity, via the WHAM benchmark).

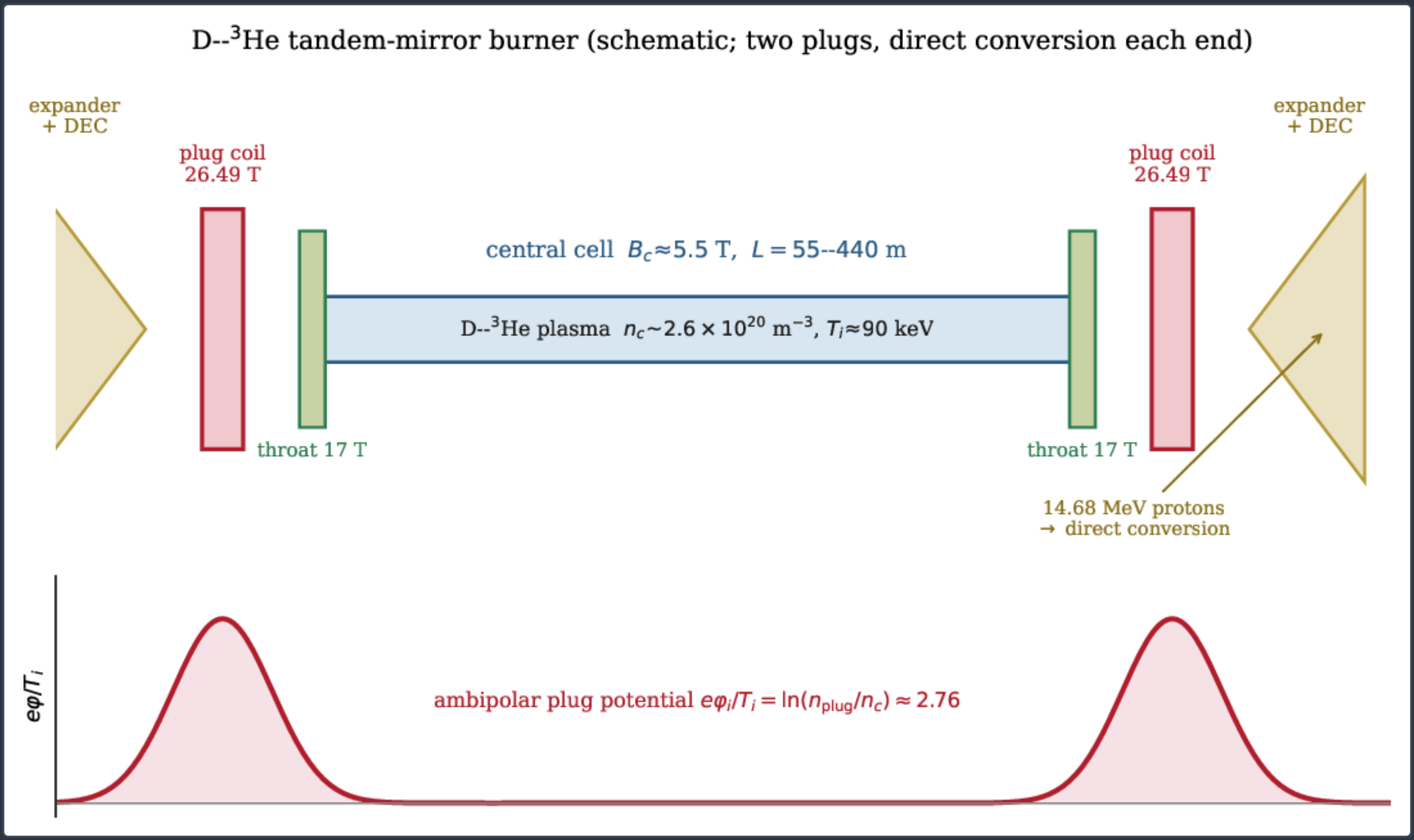

(Schematic.) The D–^{3}He tandem-mirror burner. A central cell ($B_c \approx 5.5$ T, $L = 55\text{–}440$ m) is confined between mirror throats at 17 T and a pair of high-field plug coils at 26.49 T; hot electrons and sloshing ions build the ambipolar potential well (lower panel, $e\varphi_i/T_i = \ln(n_{\text{plug}}/n_c) \approx 2.76$) that plugs the ends, and the 14.68 MeV D–^{3}He protons are direct-converted on the fanned field lines of the expanders. No data values are shown; the figure encodes structure only.

§ 3

Computational methodology: the GPU-HPC campaign

Every number in this paper is produced by the Kronos toolkit's mirror evaluator, `solve_mirror`, and its companion kinetic codes, run on the NVIDIA GPU HPC campaign (A100/H100/A10 class; hardware class only, no cost figures). This section states the discretisation, the solver, the sampling, and the reproducibility protocol.

THE 0-D EVALUATOR AND ITS SOLUTION

The power balance of §2 is a coupled nonlinear algebraic system in the state $(n_c, T_i, T_e, \varphi_i, \tau_p)$ closed by equations (2)–(8). The Maxwellian reactivity integrals $\langle \sigma v \rangle_{ab}(T_i) = \int_0^\infty \sigma_{ab}(E)\, v\, f_M(E; T_i)\, \mathrm{d}E$ are evaluated by adaptive Gauss–Legendre quadrature over the Bosch–Hale cross-sections, converged to a relative tolerance 10^{-8}; the electron temperature is obtained from the radiation-transport balance including the synchrotron closure [31]. The full system is solved by a damped Newton iteration, $x^{(k+1)} = x^{(k)} - \lambda_k J^{-1}(x^{(k)}) F(x^{(k)})$, with the Jacobian J formed analytically where the closure is smooth and by finite difference elsewhere, and the step λ_k chosen by backtracking line search until the residual $\| F\|_2 < 10^{-10}$. The converged reference point is reproducible to the full printed precision of the evaluator, $Q_E = 1.318120832690072$ (BU-L1-A1).

DESIGN-SPACE SCAN AND GLOBAL SENSITIVITY

The net-gain database (§4.2) evaluates the full balance at each node of a 5×5 grid spanning $n_e = 2.2\text{–}3.0 \times 10^{20}\ \mathrm{m}^{-3}$ and $T_i = 80\text{–}100$ keV (BU-L2-A2). The Saltelli–Sobol variance decomposition (§4.4) is computed with the SALib estimator [19,20]: a Saltelli sample of the input hypercube generates $(2d+2)N$ evaluator calls, from which the first-order indices $S_i = \mathrm{Var}_{x_i}[\mathrm{E}(Q_E \mid x_i)]/\mathrm{Var}(Q_E)$ and total-order indices S_{T_i} are estimated (HX-05). An independent 40 000-sample global Monte-Carlo (KX-L1-A5-BU) draws $(n_e, x_{^3\mathrm{He}}, T_i, \beta_c, B_m)$ over their design ranges and propagates them through the same evaluator, returning the distribution of Q_E used in §4.3. All sampling and evaluation are embarrassingly parallel and were distributed across the GPU fleet.

KINETIC CROSS-CHECKS

Three kinetic codes bound the reduced-order closure. The velocity-space microstability of the plugged distribution–the drift-cyclotron-loss-cone (DCLC) and Alfv\'en-ion-cyclotron (AIC) branches that set the warm-fill requirement–is computed by particle-in-cell simulation with WarpX [21] (BU-L2-A5, BU-L2-A7). The Fokker–Planck plug and end-loss kinetics, and the WHAM cross-check of §4.7, use a CQL3D-class mirror solver (BU-L2-A3, BU-L2-A8), with GENRAY ray tracing for the RF plug-heating deposition. These codes do not enter the 0-D anchors; they verify that the closure (3) and the warm-fill assumption are not violated at the reference point.

VERIFICATION AND REPRODUCIBILITY

The evaluator is a frozen anchor in the de-risking register [25]: an independent re-run reproduces $Q_E = 1.3181$, $P_{\mathrm{fus}} = 4298.5$ MW, $P_n = 233.95$ MW, $f_n = 5.443\%$ and $\varphi_i = 248.75$ keV to the reported precision (BU-L1-A1), and the design-space and sensitivity results (BU-L2-A2, HX-05) are regenerable from the archived scan and the figure-generation script deposited with this paper. The verification-first protocol under which the whole register is re-run and stamped is described in the companion methodology paper [34].

§ 4

Results

THE REFERENCE POWER BALANCE

Table 1 collects the frozen reference anchors reproduced by the local evaluator. The machine is neutron-lean by construction: with $f_n = 5.44\%$ the wall-averaged neutron loading is below 0.1 MW m^{-2}, and 94.6% of the fusion power appears as charged particles, of which the axial fraction is routed to the direct converters. The plug holds the design potential $\varphi_i = 248.75$ keV at a density ratio $n_{\text{plug}}/n_c = 16$, consistent with the Boltzmann closure (2) to better than one part in 10^{-3}.

QUANTITY	SYMBOL	VALUE
engineering gain	Q_E	1.318
fusion power	P_{fus}	4298.5 MW
D–^{3}He channel power	$P_{\text{D}^3\text{He}}$	3868.0 MW
neutron power	P_n	233.95 MW
neutron fraction	f_n	5.44%
plug ambipolar potential	φ_i	248.75 keV
normalised potential	$e\varphi_i/T_i$	2.764
plug density ratio	n_{plug}/n_c	16
effective mirror ratio	R_m	4.61
loss-cone half-angle	θ_{lc}	27.77°
plugged confinement time	τ_p	3.73 s
central-cell field	B_c	≈ 5.5 T
mirror-throat field	B_m	17 T
plug-coil peak field	B_{plug}	26.49 T
DEC efficiency (frozen anchor)	η_{DEC}	0.49
net electric power (440 m)	P_{net}	+850.0 MWe

Reference burner power balance: frozen anchors reproduced by the local 0-D evaluator (BU-L1-A1). Two distinct magnets appear—the 17 T mirror throat and the separate 26.49 T plug coil.

THE NET-GAIN DATABASE

To show that the reference point is representative rather than singular, the density–temperature plane was scanned on the 5×5 grid, evaluating the full balance at each node (BU-L2-A2). Every node is feasible, and *all 25 of 25 samples clear net gain*, $Q_E > 1$, over $Q_E = 1.107$–1.414 (figures 3–4, table 2). The design point ($n_e = 2.6 \times 10^{20}$ m^{-3}, $T_i = 90$ keV, $Q_E = 1.318$) lies in the interior of this box, not on a cliff edge.

Two structural features stand out. First, Q_E rises monotonically with central-cell density across the whole grid: higher density lifts the fusion power (5) faster than it raises the plugging cost. Second, at fixed density the gain peaks on an ion-temperature ridge near 85 keV–at the design density the ridge value is $Q_E = 1.375$, against 1.318 at the slightly hotter reference $T_i = 90$ keV. The reference point deliberately sits a little below the ridge, trading a few percent of gain for margin against the steepening temperature sensitivity above 90 keV, where the D–^{3}He reactivity flattens while bremsstrahlung continues to rise.

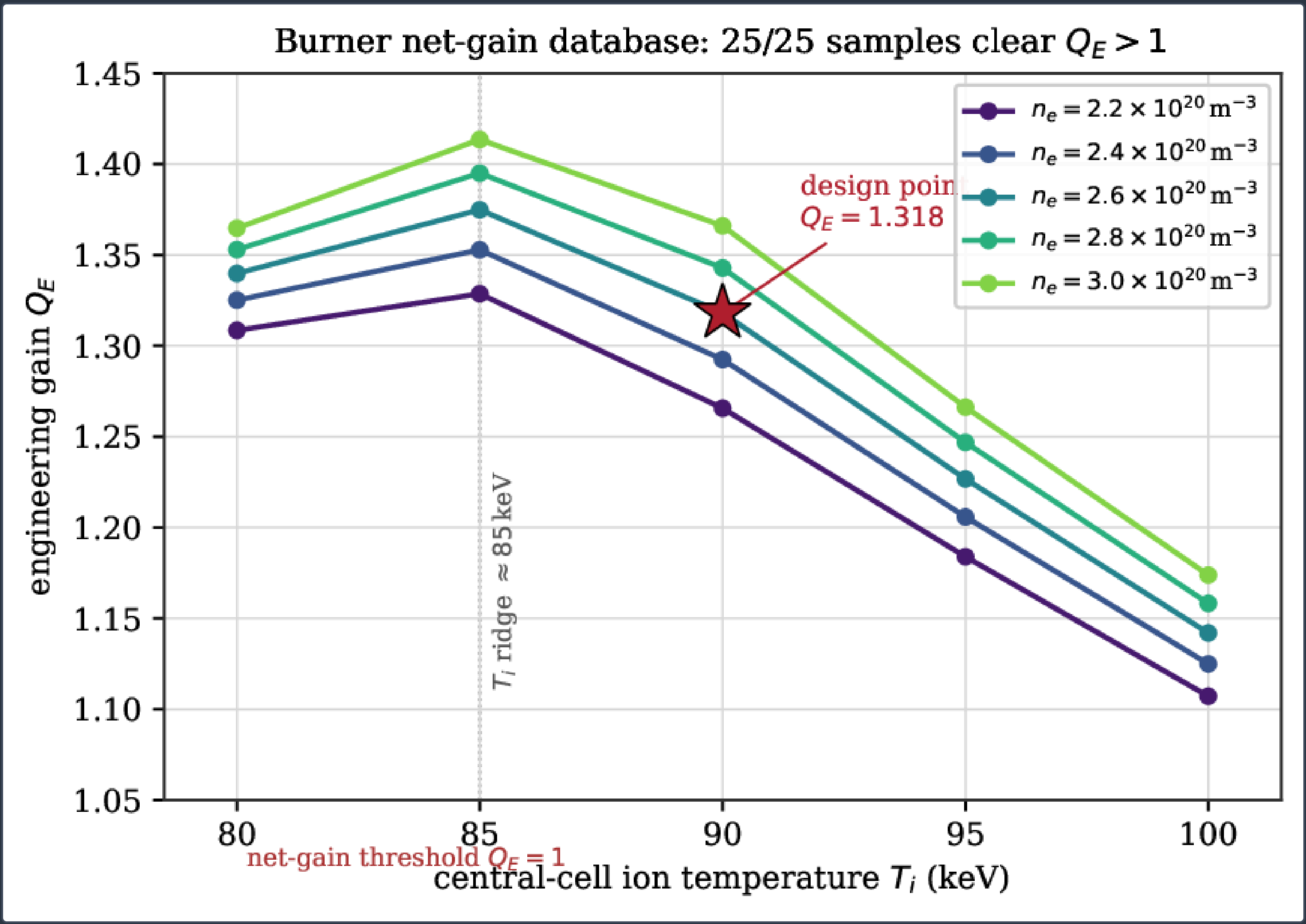

The burner net-gain database (BU-L2-A2): engineering gain Q_E versus ion temperature for five central-cell densities. Every one of the 25 feasible samples clears the $Q_E = 1$ threshold (shaded band below). The gain rises with density and peaks on a ridge near $T_i \approx 85$ keV; the star marks the canonical design point, $Q_E = 1.318$.

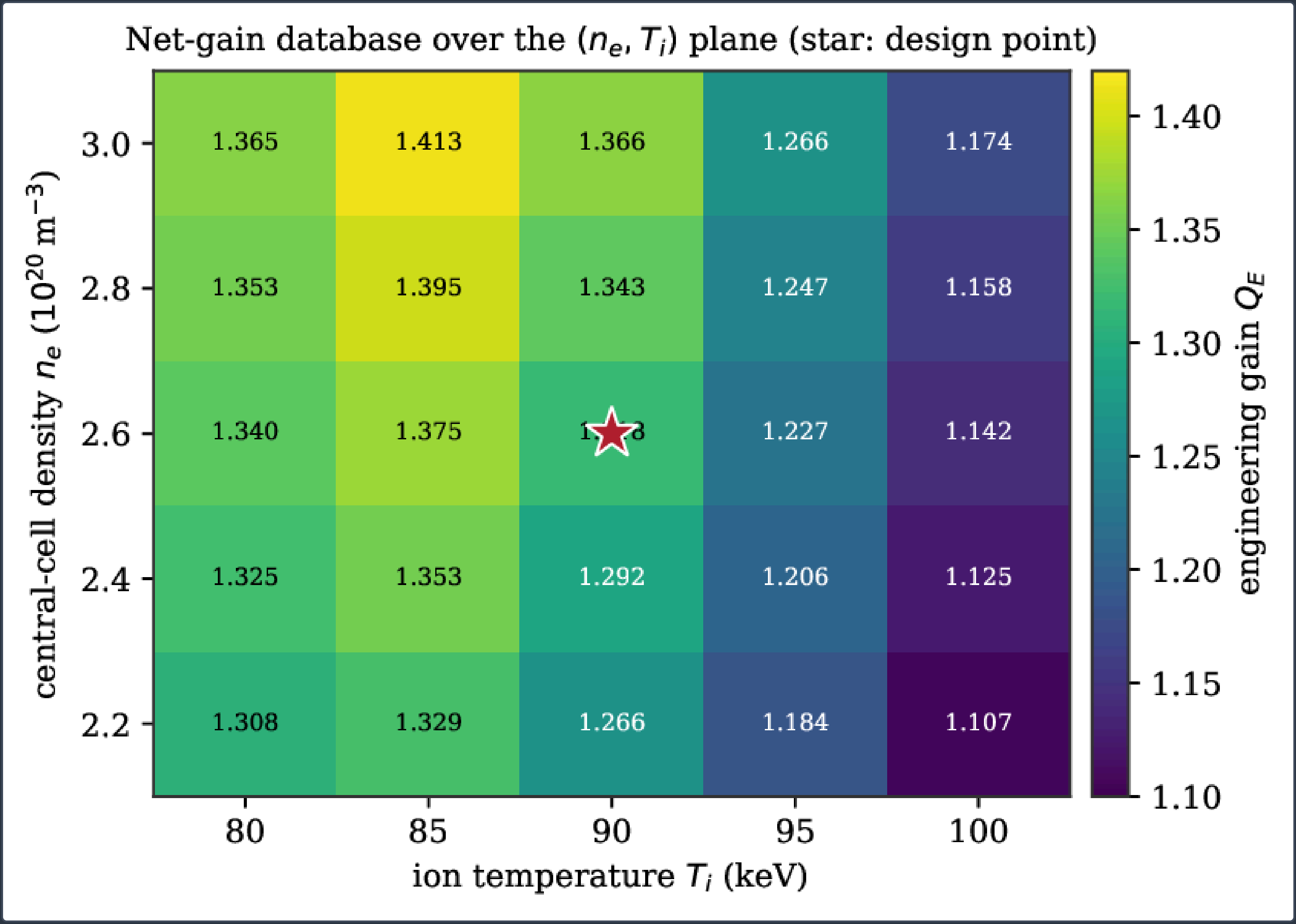

The same net-gain database as a heat map over the (n_e, T_i) plane (BU-L2-A2); the value at each grid node is printed. The gain is a smooth, single-ridged surface with the design point (star) in the feasible interior.

n_e (10^{20} m^{-3})	T_i=80	85	90	95	100
2.2	1.308	1.329	1.266	1.184	1.107
2.4	1.325	1.353	1.292	1.206	1.125
2.6	1.340	**1.375**	**1.318**	1.227	1.142
2.8	1.353	1.395	1.343	1.247	1.158
3.0	1.365	**1.414**	1.366	1.266	1.174

Net-gain database: Q_E at each grid node (BU-L2-A2). All 25 values exceed unity; boldface marks the design-density ridge value and the reference point.

GLOBAL UNCERTAINTY QUANTIFICATION

The grid scan fixes the plug density ratio; to probe robustness against simultaneous variation of all the leading inputs, an independent 40 000-sample global Monte-Carlo (KX-L1-A5-BU) draws $(n_e, x_{^3\mathrm{He}}, T_i, \beta_c, B_m)$ over their design ranges and propagates them through the evaluator. The resulting gain distribution is $Q_E = 1.317 \pm 0.14$ with $P(Q_E > 1) = 1.0$–not a single sample in forty thousand fails net gain (figure 5)–and the mean coincides with the reference anchor to three digits. The dominant correlate of Q_E in the ensemble is the central-cell β_c (correlation 0.93), foreshadowing the sensitivity decomposition below. The propagated result confirms that the net-gain box of §4.2 is not an artefact of holding other variables fixed: net gain survives correlated excursions across the whole design plane. The cross-machine uncertainty analysis of which this is the burner slice is reported in full separately [33].

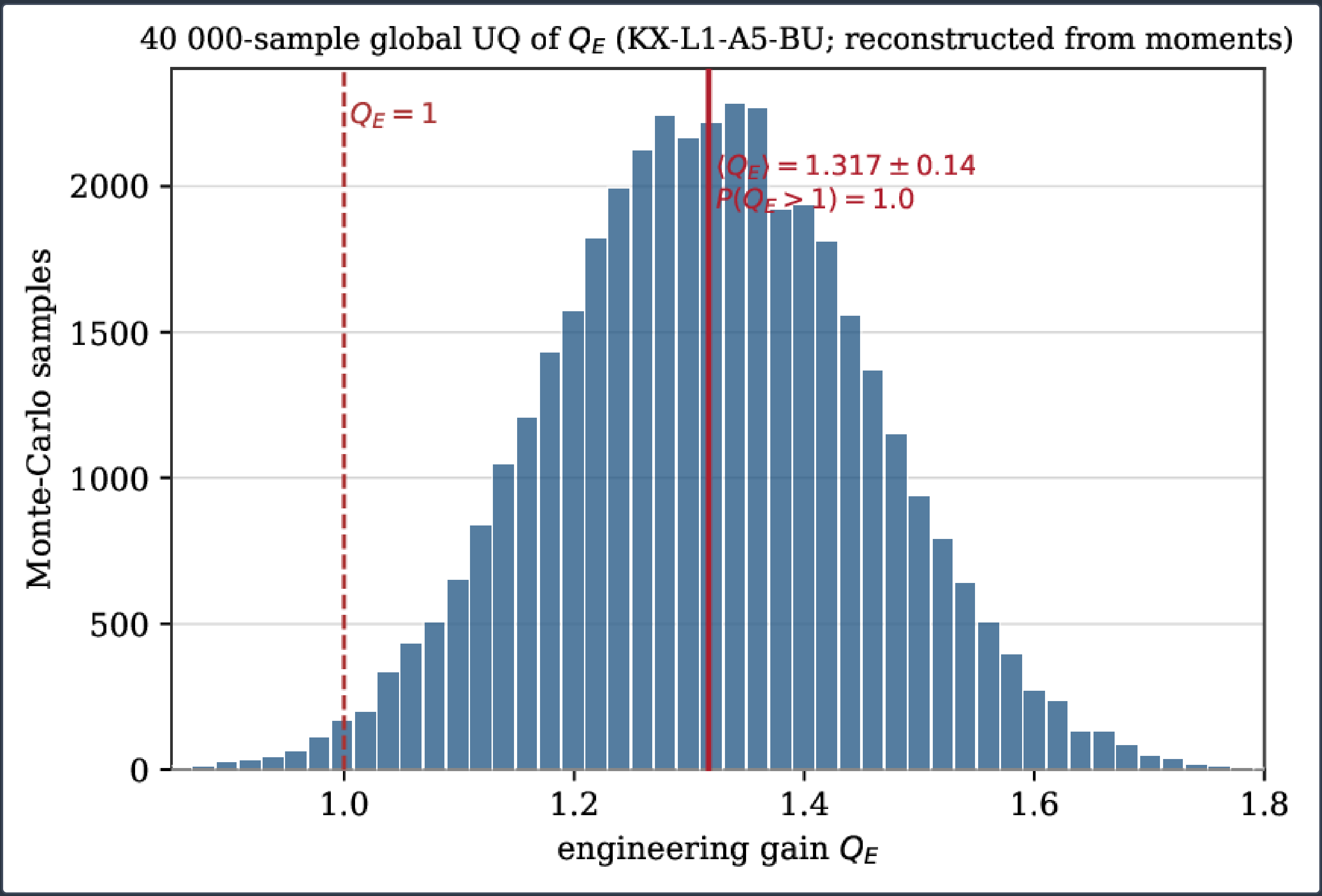

Global uncertainty quantification of the engineering gain (KX-L1-A5-BU): the distribution of Q_E over a 40 000-sample Monte-Carlo of $(n_e, x_{^3\mathrm{He}}, T_i, \beta_c, B_m)$ gives $Q_E = 1.317 \pm 0.14$ with $P(Q_E > 1) = 1.0$. The histogram is reconstructed from the frozen summary statistics; the mean coincides with the reference anchor.

WHAT DRIVES THE GATE: GLOBAL SENSITIVITY

Knowing that gain is broadly feasible, the operative question is which parameter governs it. The Saltelli–Sobol decomposition (HX-05) resolves the plug density ratio as the leading first-order driver, $S_1 = 0.41$, and central-cell β as carrying a large total-order index, $S_T = 0.87$ (figure 6). The reading is physical and follows directly from the governing equations. The plug density ratio sets the potential depth logarithmically through equation (2); the confinement, and hence the gain, then rises *exponentially* in that potential through the Pastukhov factor $\hat{\varphi}\, e^{\hat{\varphi}}$ of equation (3). Differentiating,

$$\frac{\partial \tau_p}{\partial (n_{\text{plug}}/n_c)} = \frac{\partial \tau_p}{\partial \hat{\varphi}} \frac{\partial \hat{\varphi}}{\partial (n_{\text{plug}}/n_c)} = \left[\tau_{ii}\sqrt{\pi}\, g(R_m)(1+\hat{\varphi})e^{\hat{\varphi}}\right] \cdot \frac{1}{n_{\text{plug}}/n_c},$$

so a fractional change in the density ratio moves the confinement by the large factor $(1+\hat{\varphi}) \approx 3.8$ times the exponential enhancement–the strongest single lever in the model. Central-cell β enters largely through interactions ($S_T \gg S_1$ for β): it multiplies the fusion power density that the plug then confines, rather than adding an independent contribution, so plug performance and central-cell pressure must be co-designed. The practical consequence is that the high-field plug coil is the pacing subsystem of the burner program, which is why its structural and quench qualification is carried as a dedicated study [27].

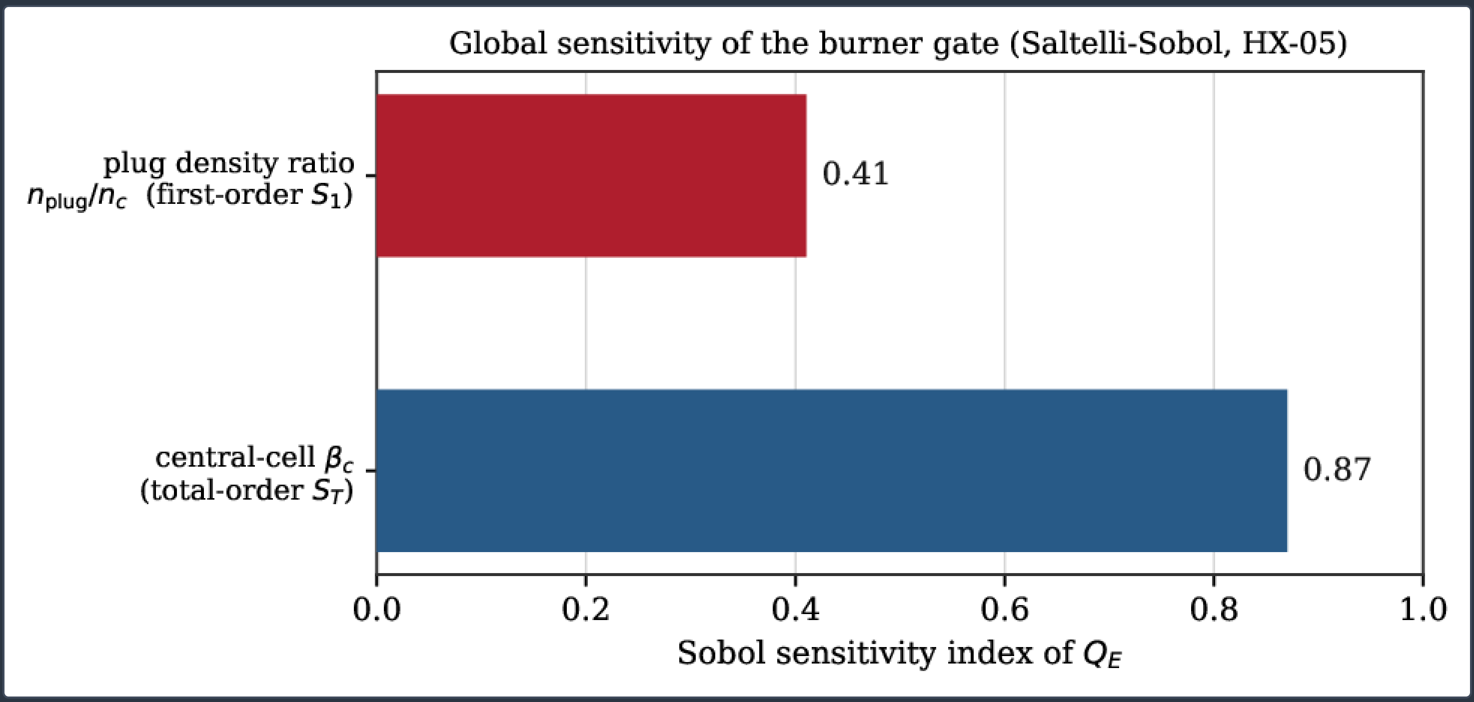

Global sensitivity of the burner engineering gain (Saltelli–Sobol, HX-05). The plug density ratio is the leading first-order driver ($S_1 = 0.41$); central-cell β enters largely through interactions ($S_T = 0.87$), consistent with the analytic lever of equation (10).

THE DIRECT-CONVERSION EFFICIENCY LADDER

The frozen DEC anchor $\eta_{\mathrm{DEC}} = 0.49$ is deliberately conservative. Direct conversion of the 14.68 MeV proton channel (6) has an established performance ladder [3,13,28]: an engineering floor near 0.56, the Moir–Barr reference-design value 0.70, and an ideal proton-only ceiling of 0.85 (BU-SX-01/03). The reference power flow that closes at $Q_E = 1.318$ ($P_{\mathrm{out}} = 3522.0$ MWe, net +850.0 MWe) adopts the design value; the frozen anchor 0.49 is quoted as a pessimistic bound below the floor. Because η_{DEC} enters equation (8) linearly through the large charged-particle term, net gain requires $\eta_{\mathrm{DEC}} \gtrsim 0.52$ (BU-L1-A10), and the ladder (figure 7) makes explicit that the reference design sits comfortably above that crossover while the conservative anchor sits just below it. The DEC efficiency is therefore a genuine edge of the operating window–treated quantitatively rather than assumed away–and the converter architecture that realises the design value is developed in the companion converter studies [28].

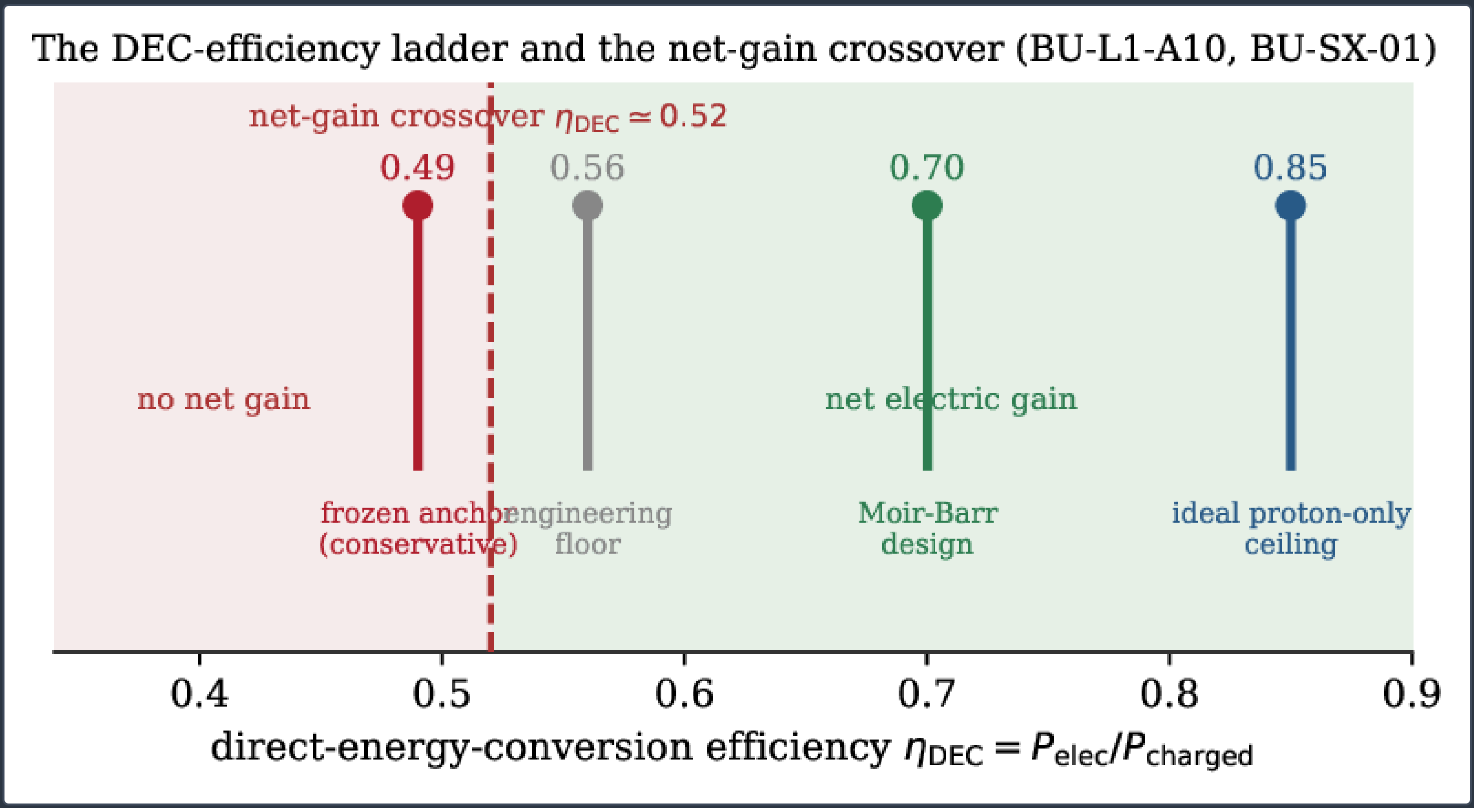

The direct-energy-conversion efficiency ladder and the net-gain crossover (BU-L1-A10, BU-SX-01). Net electric gain requires $\eta_{\mathrm{DEC}} \gtrsim 0.52$; the frozen conservative anchor (0.49), the engineering floor (0.56), the Moir–Barr design value (0.70) and the ideal proton-only ceiling (0.85) are marked.

ONE PHYSICS, TWO HOUSINGS: POWER-CLASS SCALING

The design space extends along a third axis–the central-cell length–because the two burner housings share identical plug and confinement physics and differ only in scale. The balance closes at $Q_E = 1.309$ and net $+104.2$ MWe for the 55 m Aegis unit ($P_{\text{fus}} = 537.3$ MW, $P_{\text{out}} = 441.1$ MWe, $P_{\text{in}} = 336.9$ MWe, recirculation 0.764; AG-L1-A1) and at $Q_E = 1.318$ and net $+850.0$ MWe for the 440 m reference unit, so the net power scales essentially linearly with length while the engineering gain is nearly length-invariant (figure 8). The near-constant recirculation fraction ($P_{\text{in}}/P_{\text{out}} \approx 0.76$) across this factor-of-eight range in length is the signature of an open system whose gain is set by the plug rather than by size: lengthening the central cell adds fusion power and export power in the same proportion. This is the physical basis for a single design serving both a compact forward-base unit [26] and a large data-centre unit.

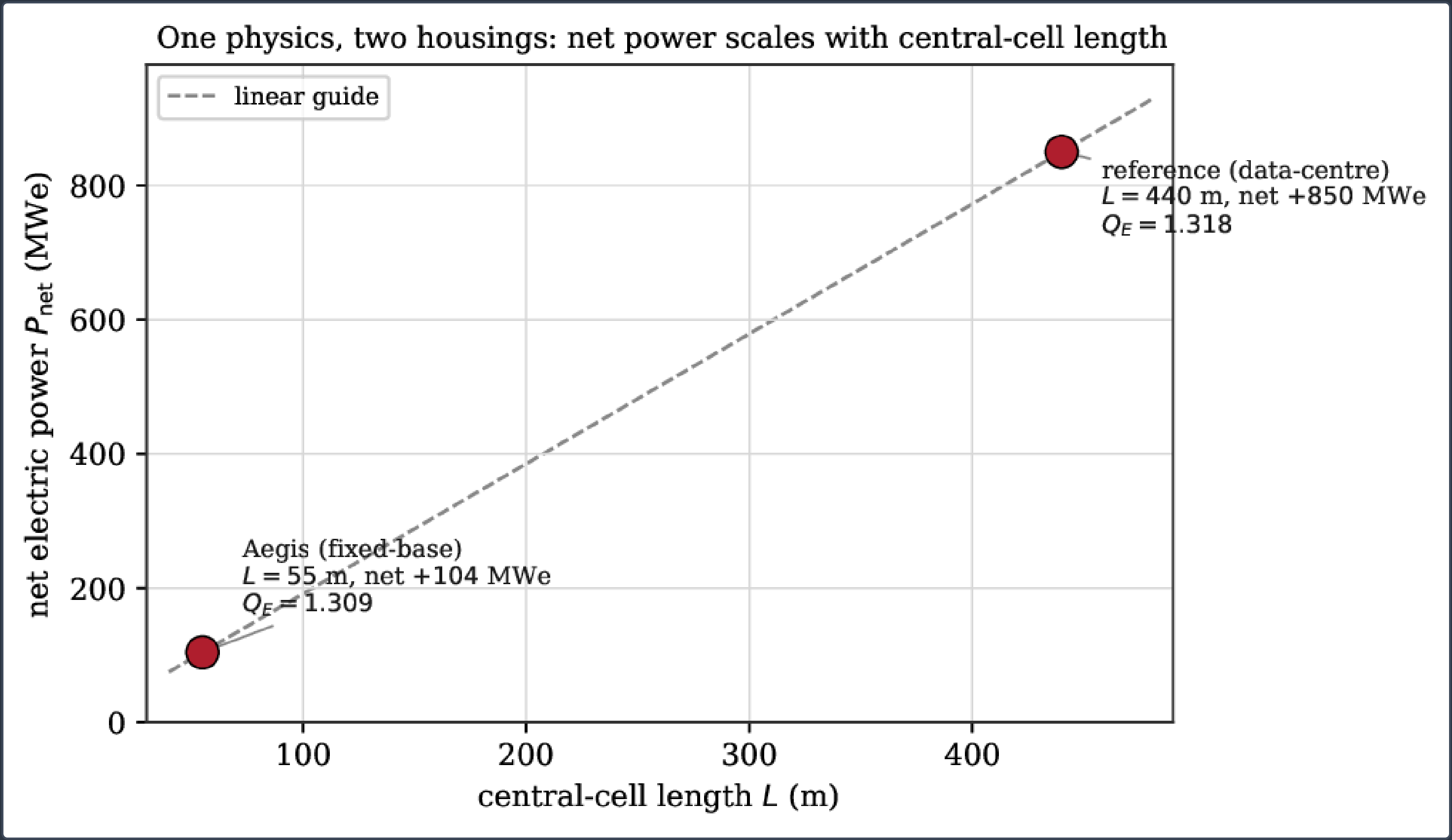

One physics, two housings (AG-L1-A1, BU-L1-A1): net electric power scales with central-cell length from the 55 m Aegis unit ($+104.2$ MWe, $Q_E = 1.309$) to the 440 m reference unit ($+850.0$ MWe, $Q_E = 1.318$), at nearly constant engineering gain and recirculation fraction.

THE WHAM BENCHMARK

The one operating machine relevant to this model class is the Wisconsin HTS Axisymmetric Mirror (WHAM) [16,17], a 17 T HTS simple mirror–the exact field regime the burner throats assume. Benchmarking the Kronos mirror model against WHAM has a clear, honest result (table 3, figure 9). Where a measurement exists, the model agrees: the fields and geometry match within $\sim 5\%$ (central field 0.86 T published versus 0.828 T modelled; vacuum mirror ratio 19.8 versus 20.5), the kilovolt-class ambipolar potential and its $e\varphi_e/T_e \approx 5$ are reproduced, and the D–D neutron rate is bracketed within a factor of order six (1.1×10^{13}–1.0×10^{14} s^{-1} modelled versus 6.2×10^{13} s^{-1} published). The unplugged confinement scaling is likewise reproduced: the Pastukhov confinement time rises with mirror ratio from ≈ 2.3 μs at $R_m \sim 2$ to ≈ 15 μs at $R_m \sim 12$ (figure 9a).

The one channel that disagrees is the absolute confinement time in WHAM's regime, and it disagrees *conservatively*. WHAM is an unplugged simple mirror operating at $e\varphi_i/T_i \sim 0.03$–0.07, far below the Pastukhov plugging threshold of $\simeq 0.5$ (figure 9b); the closure (3) is not valid there, and applied outside its domain it underpredicts the measured confinement by two to three orders (modelled $\tau_p = 73$ μs versus ~ 7.2 ms derived). The disagreement is therefore never optimistic: the model is pessimistic exactly where it does not apply. WHAM does not operate a Pastukhov plug, so it cannot by itself validate the plugged, net-gain branch on which the burner depends; the burner design point sits at $e\varphi_i/T_i = 2.764$, deep in the plugged regime, with $\tau_p = 3.73$ s. The benchmark thus delivers what a benchmark should: it confirms the code where a measurement exists, and it localises the remaining physics to one well-posed question–the quantitative performance of the high-field plug–that a plugged-mirror experiment is built to answer.

QUANTITY	WHAM (MEASURED / DERIVED)	KRONOS MODEL
central field B_0	0.86 T	0.828 T ($< 5\%$)
vacuum mirror ratio	19.8	20.5 ($< 5\%$)
normalised potential $e\varphi_e/T_e$	≈ 5	reproduced
D–D neutron rate (s^{-1})	6.2×10^{13}	1.1×10^{13}–1.0×10^{14}
$e\varphi_i/T_i$ (regime)	0.03–0.07 (unplugged)	below the 0.5 plug threshold
confinement τ	~ 7.2 ms (derived)	73 μs (conservative, out of domain)
3l*Burner design point (plugged):* $e\varphi_i/T_i = 2.764$, $\tau_p = 3.73$ s		

WHAM benchmark of the Kronos mirror model (BU-L2-A3). The model reproduces the measured fields, potential and neutron rate; the absolute confinement disagrees only in the *unplugged* regime, where the Pastukhov closure is out of its validity domain and errs conservatively.

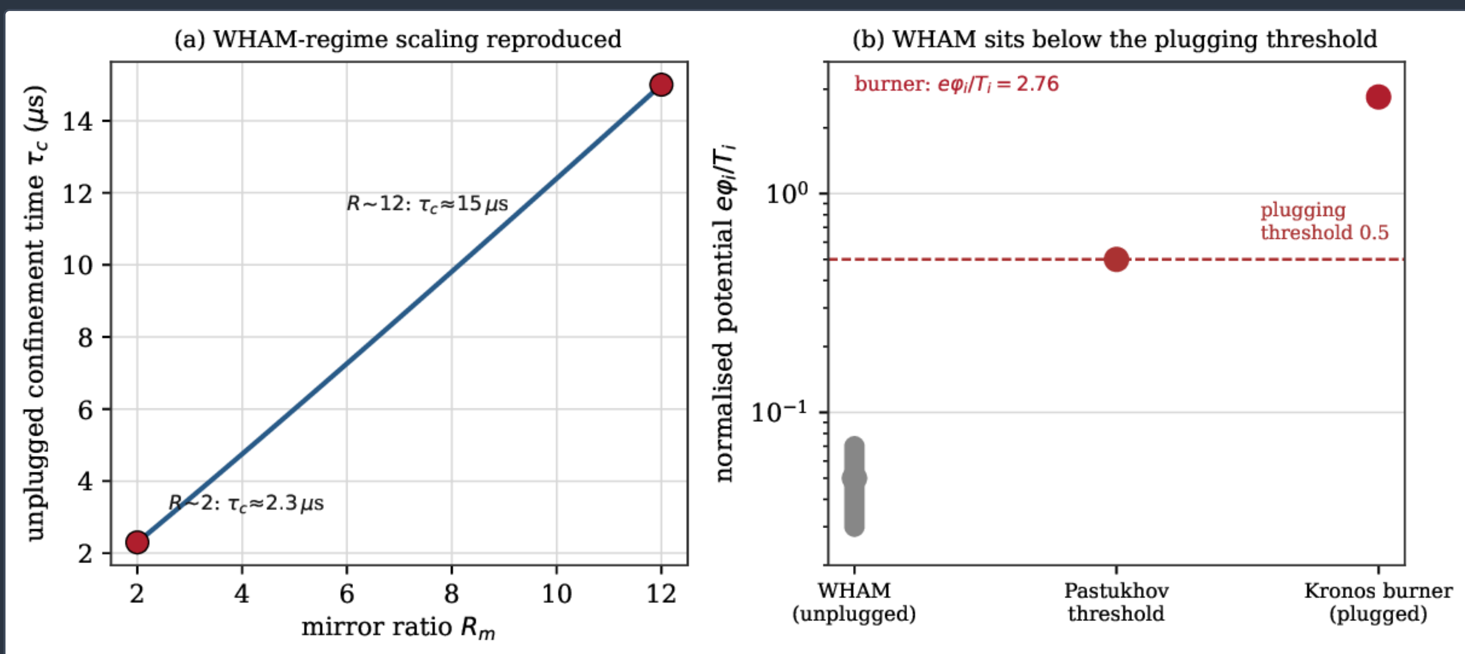

The WHAM benchmark (BU-L2-A3). **(a)** The unplugged confinement scaling is reproduced: τ_c rises with mirror ratio from ≈ 2.3 μs at $R_m \sim 2$ to ≈ 15 μs at $R_m \sim 12$. **(b)** WHAM operates at $e\varphi_i/T_i \sim 0.03$–0.07, below the Pastukhov plugging threshold (0.5); the burner design point sits at 2.764, deep in the plugged regime the benchmark cannot yet reach.

§ 5

Discussion

The six results compose into a coherent design case. The reference balance closes at net electric gain with a neutron-lean, directly converted output (§4.1); the net-gain database and its 40 000-sample uncertainty quantification show that gain is the interior of a broad box rather than a fragile optimum, with a deliberate margin against the temperature ridge (§§4.2–4.3); the global sensitivity ranks the plug density ratio and its coupling to central-cell β as the physical levers, tying the ranking analytically to the Pastukhov exponential (§4.4); the DEC ladder places the conversion efficiency edge of the window quantitatively (§4.5); and the two-housing scaling shows one physics serving a factor-of-eight range in machine length at nearly constant gain (§4.6).

Quantitatively, the picture is consistent with the published tandem-mirror and advanced-fuel literature. The plugging mechanism itself–a positive ambipolar potential built by a dense end plug–is the same one demonstrated at kilovolt scale on TMX-U and GAMMA-10 [10,11]; the burner simply asks a high-field REBCO plug to hold a deeper potential ($e\varphi_i/T_i = 2.764$) than those experiments reached, which is precisely the extrapolation the sensitivity analysis flags as load-bearing. The net-electric, high-gain tandem-mirror configuration is in the spirit of the simplified high-field concept of Fowler, Moir and Simonen [12], but the present $Q_E = 1.318$ is a conservative engineering gain that already includes recirculation and a below-floor DEC anchor, rather than a physics Q. The DEC ladder floor and design values ($0.56/0.70$) sit within the range measured on the Moir–Barr converters [3,13], and the neutron fraction $f_n = 5.44\%$ is the expected order for a D–^{3}He system with a modest D–D side burn, consistent with the advanced-fuel confinement analyses of Nevins and of Kulcinski and Santarius [14,15]. The WHAM benchmark then draws the boundary of what is measured versus modelled and places the burner's remaining physics risk on one identified checkpoint rather than diffusing it across the machine. A compact burner with a mapped, sensitivity-ranked operating window and a single, testable open question is a well-posed engineering program.

§ 6

Limitations

One honest gate bounds the claims. The plugged, net-gain branch has not been validated against a plugged-mirror measurement: WHAM benchmarks only the *unplugged* regime ($e\varphi_i/T_i \sim 0.03$–0.07, below the 0.5 plug threshold), so the quantitative performance of the high-field plug at the design potential $e\varphi_i/T_i = 2.764$ is the one open experimental item. It is addressed by the 26.49 T plug-coil qualification [27] and, ultimately, by a plugged end-cell test. Two secondary caveats follow the same line: the central-cell $\beta_c = 0.55$ is an assumed input rather than an MHD-solved equilibrium (its stability is treated in the companion transport-and-MHD study), and the warm-fill that stabilises the DCLC loss-cone leaves a residual AIC branch that is a plug-gate caveat, not a showstopper [30]. The database and sensitivity results are 0-D on a verified evaluator; higher-dimensional kinetic effects are carried in the companion end-cell and recirculation studies [32].

§ 7

Conclusion

The Kronos D–^{3}He tandem-mirror burner reaches net electric gain at $Q_E = 1.318$ and holds $Q_E > 1$ across all 25 samples of a broad density–temperature box ($Q_E = 1.107$–1.414), with a $40\,000$-sample global Monte-Carlo returning $Q_E = 1.317 \pm 0.14$ at $P(Q_E > 1) = 1.0$. Global sensitivity ranks the plug density ratio as the leading driver ($S_1 = 0.41$), coupled to central-cell β ($S_T = 0.87$), and we show this follows analytically from the exponential Pastukhov dependence on $\ln(n_{\text{plug}}/n_c)$–identifying the high-field plug as the subsystem to engineer first. One physics scales across two housings, from $+104$ MWe net at 55 m to $+850$ MWe net at 440 m, at nearly constant gain and recirculation. A WHAM benchmark validates the model in the unplugged regime–matching fields, potential and neutron rate–and isolates the plugged-branch plug performance as the single experimental checkpoint. The burner enters detailed design with a demonstrated, sensitivity-mapped operating window and one well-posed open question.

Acknowledgments tocsectionAcknowledgments Part of the Kronos Fusion Energy 2026 design series. The authors thank the Kronos physics de-risking programme for the frozen result set underlying every quantitative claim, and the NVIDIA GPU HPC campaign for the computational resources.

Reproducibility. The reference power balance (BU-L1-A1), the 25-point net-gain database (BU-L2-A2), the Saltelli–Sobol indices (HX-05), the 40 000-sample global uncertainty quantification (KX-L1-A5-BU), the DEC ladder (BU-L1-A10, BU-SX-01/03), the two-housing scaling (AG-L1-A1) and the WHAM benchmark (BU-L2-A3) are frozen anchors in the Kronos Physics De-Risking Register and are regenerable from the mirror evaluator, the scan scripts, and the figure-generation script archived with this paper. This paper is archived at its DOI doi:10.5281/zenodo.22645911; official version: https://www.kronosfusionenergy.com/publications/tandem-mirror-design-space-mapping-for-a-d-he-burner-0-.html and at its official page https://www.kronosfusionenergy.com/publications/tandem-mirror-design-space-mapping-for-a-d-he-burner-0-.html; the de-risking register is archived at doi:10.5281/zenodo.22133057.

Data availability tocsectionData availability The design-space scan table, the power-balance outputs, the sensitivity indices and the WHAM benchmark values used for the figures are archived with the deposit at doi:10.5281/zenodo.22645911 and reference the Kronos 2026 series. All quantitative values trace to the register [25] by the serial identifiers cited inline. Any economic analysis is reported separately and is not part of the public deposit.

Competing interests tocsectionCompeting interests Provisional patent applications relating to aspects of this work have been filed.

tocsectionReferences

APPARATUS

Portfolio, People & Record

The intellectual-property estate, the people who built it, the limitations that gate it, and the sources it rests on.

1	4	40	27
GRANTED PATENT	2026 PROVISIONALS	TEAM MEMBERS	2022 PROVISIONALS

INTELLECTUAL PROPERTY

The patent portfolio

The estate spans a granted high-field magnet patent, pending utility and 2026 provisional filings that map to the two products, a digital-twin control provisional, a registered trademark application, and the original 2022 provisional family. Every patentable disclosure in the five-paper arXiv drop was protected **before** publication: the breeder and burner provisionals were filed 1–2 August, and a publication-gap omnibus filing the evening before the drop swept up the DEC, plasma-control, and REBCO-winding matter of the three otherwise-unprotected papers. Patent numbers and application serials are matters of public record; claim scope is summarised, not reproduced.

GRANTED & PENDING UTILITY

US 12,009,112	High-field tilted graded-REBCO magnet architecture (KRONO-002A) · *app. 17/878,550*	GRANTED
US 17/878,507	Core device / method (KRONO-001A) · *utility*	PENDING

2026 PROVISIONAL FILINGS — MAPPED TO THE PRODUCTS

64/124,209	Hyperion — spherical-tokamak tritium / helium-3 foundry · *breeder · filed Aug 2026*	FILED
64/124,220	Aegis / MetroVolt — synchrotron-cutoff, fuel-selection & plug-winding · *generator · filed Aug 2026*	FILED
64/115,167	KRONOS-CTRL digital-twin plant control · *provisional · filed Jul 2026*	FILED
64/005,440	Integrated spherical-tokamak fusion architecture · *early integrated-architecture filing · filed Mar 2026*	FILED
64/105,530	Negative-triangularity spherical-tokamak architecture · *foundational ST filing · filed Jul 2026*	FILED
64/128,097	Publication-gap omnibus — quasineutral two-species expander DEC · provenance-gated / latency-split plasma control · as-built high-field winding & conductor architecture · *filed 7 Aug 2026, the evening before the arXiv drop*	FILED

TRADEMARK & ORIGIN

FTK-98801894	Kronos Fusion Energy — trademark application	FILED
KR-2022-*	Original provisional family (KR-2022-00001 … 00027) · *27 filings, 2022*	PRIORITY

The narrow, defensible magnet novelty — the specific conductor and the digital-twin winding optimisation, not high-field REBCO as a category — is the commercial core that can earn ahead of any Q > 1 milestone, with markets in fusion magnet supply, MRI/NMR, accelerators, and proton therapy. The claim is scoped honestly: the high field is a *system field* result, not a stand-alone-coil record; the small-bore plug coil is structurally infeasible as a bare winding but resolved by a stress-managed structural shield (feasible-pending-FEA); and the winding-tape experiment returned a *null result*. The value is the method, not a field record.

THE TEAM

Founding partners, board, advisors & auditors

Kronos is built by a bench of advanced-fuel-fusion, high-field-magnet, direct-conversion, and materials specialists, with a board and operations team drawn from defense, national laboratories, and industry. Dates are shown as ranges; where a tenure has ended or is term-ending, the range says so.

FOUNDING PARTNERS — SCIENCE

Dr. Gerald Kulcinski
Co-Founder · Helium-3 & Advanced-Fuel Fusion
UW–Madison · 2023–Present

Dr. Carl Weggel
Chief Scientist / S.M.A.R.T. Design
MIT Alcator Program · 2022–Present

Dr. Robert J. Weggel
Magnetic Field Design
MIT Magnet Lab · 2022–Present

BOARD

Priyanca Ford
Founder & CEO · Executive Board
2022–Present

Bandel Carano
Finance / Strategy
Oak Investment Partners / Stanford · 2025–2026

Patrick Schweiger
Fusion Device Engineering
Oklo / CFS / TerraPower · 2025–Present

SCIENTIFIC ADVISORS

Dr. Steven O. Dean
Fusion Policy & History
DOE / Fusion Power Associates · 2025–Present

Dr. Patrick H. Diamond
Plasma Turbulence & Transport
UC San Diego · 2025–Present

Dr. Jack J. Dongarra
HPC & Numerical Algorithms
Turing Award · 2025–Present

Dr. Nasr M. Ghoniem
Chief Material Scientist
UCLA · 2025–Present

Dr. Siegfried Glenzer
Plasma Physics & Laser Fusion
Stanford / SLAC · 2022–Present

Dr. David A. Hammer
Pulsed-Power Fusion
Cornell · 2025–Present

Dr. Donald A. Spong
Plasma Theory & Confinement
ORNL · 2025–Present

Dr. Curtis Smith
Risk Assessment & Nuclear PRA
MIT / Idaho National Lab · 2025–Present

RADM (Ret.) David Goggins
Naval Engineering & Power-Plant Design
U.S. Navy · 2023–2026

Dr. Konstantin Batygin
Mathematician
Caltech · 2022–2025

Dr. Ruben Fair
Magnet Design / ITER Liaison
PPPL / Jefferson Lab · 2022–2025

Dr. Paul S. Weiss
Materials & Nanotechnology
UCLA · 2022–2025

SCIENTIFIC AUDITORS

Dr. Wilfred A. Cooper
Plasma Equilibrium Theory
EPFL / Swiss Plasma Center · 2025–Present

Dr. Ahmed Hassanein
Plasma–Material Interactions
Purdue / Argonne · 2025–Present

Dr. Patrick E. Hopkins
Extreme Thermal Materials
U. of Virginia · 2025–Present

Dr. Peter Hosemann
Materials Joining & Structural Integrity
UC Berkeley · 2025–Present

Dr. Travis W. Knight
Advanced Nuclear Fuels & Systems
U. of South Carolina · 2025–Present

Dr. Philippe Lebrun
Cryogenics & Magnet Cooling
CERN · 2025–Present

Dr. Nitendra Singh
Nuclear Safety & Fuel Cycle
ITER · 2025–Present

Dr. Guido Van Oost
Magnetic Confinement & Fusion Systems
Ghent University · 2025–Present

Dr. Gary S. Was
Radiation Materials & Structural Integrity
U. of Michigan · 2025–Present

Dr. Ray Sedwick
Direct Energy Conversion
U. of Maryland · 2025

OPERATIONS

Michael Laughlin
Chief Operating Officer
2022–Present

Martin Owens
Chief Strategy Officer
LANL / GE Hitachi · 2022–Present

MG (Ret.) Paul Pardew
Chief Contracting Officer
Army Contracting Command · 2022–Present

David Beck
Fusion Commercialization
U.S. Space Force · 2024–Present

Sushma Bhatia
Environmental & Legislative
Google · 2022–Present

Michael De Frenza
Technology Licensing
2023–Present

MG (Ret.) Robin L. Fontes
Cybersecurity & Defense
Army Cyber Command · 2022–Present

Vijay Gehani
Supply Chain & Components
INOX India · 2024–Present

Jon Michel Greenwood
IT & AI Infrastructure
Live Nation · 2023–Present

Brian C. O'Neill
National Security
CIA / ODNI · 2022–Present

Gen. (Ret.) Gustave F. Perna
DoD Liaison
Operation Warp Speed · 2022–2023

Andrea Romero
Marketing Lead
2022–Present

Legal counsel is retained; those roles are held on the internal roster and are not listed here.

SOURCES

References

1. R F Post, The magnetic mirror approach to fusion, *Nucl. Fusion* **27** 1579 (1987).
2. D D Ryutov, Open-ended traps, *Sov. Phys. Usp.* **31** 300 (1988).
3. R W Moir and W L Barr, Venetian-blind direct energy converter for fusion reactors, *Nucl. Fusion* **13** 35 (1973).
4. G I Dimov, V V Zakaidakov and M E Kishinevsky, Thermonuclear confinement with twin mirror systems, *Sov. J. Plasma Phys.* **2** 326 (1976).
5. T K Fowler and B G Logan, The tandem mirror reactor, *Comments Plasma Phys. Control. Fusion* **2** 167 (1977).
6. D E Baldwin and B G Logan, Improved tandem mirror fusion reactor, *Phys. Rev. Lett.* **43** 1318 (1979).
7. V P Pastukhov, Collisional losses of electrons from an adiabatic trap in a plasma with a positive potential, *Nucl. Fusion* **14** 3 (1974). doi:10.1088/0029-5515/14/1/001
8. R H Cohen, T D Rognlien and D E Baldwin, Collisional loss of electrostatically confined species in a magnetic mirror, *Nucl. Fusion* **18** 1229 (1978).
9. F Najmabadi, R W Conn and R H Cohen, Collisional end loss of electrostatically confined particles in a magnetic mirror field, *Nucl. Fusion* **24** 75 (1984).
10. T C Simonen *et al*, Operation of the tandem mirror plasma experiment with thermal barriers, *Phys. Rev. Lett.* **50** 1668 (1983).
11. T Cho *et al*, Observation and control of transverse energy-transport barrier due to the formation of an energetic-electron layer in the GAMMA 10 tandem mirror, *Phys. Rev. Lett.* **94** 085002 (2005).
12. T K Fowler, R W Moir and T C Simonen, A new simpler way to obtain high fusion power gain in tandem mirrors, *Nucl. Fusion* **57** 056014 (2017).
13. W L Barr and R W Moir, Test results on plasma direct converters, *Nucl. Technol./Fusion* **3** 98 (1983).
14. W M Nevins, A review of confinement requirements for advanced fuels, *J. Fusion Energy* **17** 25 (1998).
15. G L Kulcinski and J F Santarius, Advanced fuels under debate, *Nature* **396** 724 (1998).
16. D Endrizzi *et al*, Physics basis for the Wisconsin HTS Axisymmetric Mirror (WHAM), *J. Plasma Phys.* **89** 975890501 (2023).
17. J Egedal, D Endrizzi, C B Forest and T K Fowler, Fusion by beam ions in a low collisionality, high mirror ratio magnetic mirror, *Nucl. Fusion* **62** 126053 (2022).
18. H-S Bosch and G M Hale, Improved formulas for fusion cross-sections and thermal reactivities, *Nucl. Fusion* **32** 611 (1992).
19. A Saltelli *et al*, Variance based sensitivity analysis of model output: design and estimator for the total sensitivity index, *Comput. Phys. Commun.* **181** 259 (2010). doi:10.1016/j.cpc.2009.09.018
20. I M Sobol′, Global sensitivity indices for nonlinear mathematical models and their Monte Carlo estimates, *Math. Comput. Simul.* **55** 271 (2001).
21. J-L Vay *et al*, Warp-X: a new exascale computing platform for beam–plasma simulations, *Nucl. Instrum. Methods Phys. Res. A* **909** 476 (2018).
22. S Hahn *et al*, 45.5-tesla direct-current magnetic field generated with a high-temperature superconducting magnet, *Nature* **570** 496 (2019). doi:10.1038/s41586-019-1293-1
23. B N Sorbom *et al*, ARC: a compact, high-field, fusion nuclear science facility and demonstration power plant with demountable magnets, *Fusion Eng. Des.* **100** 378 (2015). doi:10.1016/j.fusengdes.2015.07.008
24. W L Oberkampf and T G Trucano, Verification and validation in computational fluid dynamics, *Prog. Aerosp. Sci.* **38** 209 (2002).
25. P I Ford, *The Physics De-Risking Register: Gate-by-Gate Evidence for a Compact Spherical-Tokamak Breeder and Its D–^{3}He Tandem-Mirror Burners*, Kronos Fusion Energy 2026 series. doi:10.5281/zenodo.22133057; register deposit doi:10.5281/zenodo.22645689.
26. P I Ford and G L Kulcinski. *The Aegis Forward-Base Burner: Q_E Closure. Plug Requirement. and Mirror Confinement in an*

COLOPHON

How this document was made

The Kronos Fleet — Combined Editorial, 2026 is set in **Fraunces** (display), **Gelasio** (text), and **IBM Plex Mono** (data & equations), carried forward from the Kronos editorial design system.

The figures are rendered at 300 dpi from the deposited generator scripts; the document is composed as a single self-contained file with embedded fonts and imagery, paginated to US Letter, and rendered to PDF through a headless Chromium engine in matched light and dark editions.

Every headline quantity carries an evidence class; withdrawn and restated values are marked as such. Nothing herein is frozen beyond the founder-approved Tier-A set.

Explore it live — turn the interactive 3-D model, run the deposited solvers in the physics validator, and watch the companion film series.

LEGAL NOTICE

Notice, status, and distribution

Conceptual design & simulation study. This document reports a conceptual design and simulation study. It is not a construction commitment, a safety-analysis report, a regulatory filing, or an offer of securities. Forward-looking statements — schedules, costs, market sizes, and performance — are estimates subject to the limitations set out in the Simulations part and may change.

Numbers and their classes. Quantities are reported with evidence classes and case labels; modelled, assumed, and requirement-class values are identified as such and are not to be quoted without their labels.

Public edition. This edition carries the physics and design only; all financial, funding, and defense-commercial content has been removed for public distribution. The scientific text corresponds to the arXiv and journal submissions.

THE 2026 KRONOS SERIES

One programme, many papers

This editorial is one paper in the Kronos 2026 series — a real fusion company's complete, reproducible physics record for a spherical-tokamak breeder and its low-neutron D–^{3}He tandem-mirror burners. Every headline number is a frozen anchor in the Physics De-Risking Register.

Explore the whole programme: the De-Risking Register, the interactive 3-D model, and the physics validator.

KRONOS FUSION ENERGY

Tandem-Mirror Design-Space Mapping for a D–^{3}He Burner: 0-D Power Balance Benchmarked against WHAM and the Pastukhov-Plug Operating Point

A real fusion company building real machines. Explore the science, live.

Zenodo · doi:10.5281/zenodo.22645911

Read on kronosfusionenergy.com

The Physics De-Risking Register